Structural, electronic and dielectric properties of carbon nanotubes interacting with Co nanoclusters

Icare Morrot-Woisard, Emile Nguyen, Nicolas Vukadinovic, Mauro Boero

Carbon Trends 17 (2024) 100410

Contents lists available at ScienceDirect

Carbon Trends

journal homepage: www.elsevier.com/locate/cartre

Structural, electronic and dielectric properties of carbon nanotubes interacting with Co nanoclusters

Icare Morrot-Woisard [a], Emile K. Nguyen [a], Nicolas Vukadinovic [b], Mauro Boero [c,*]

[a] University of Strasbourg - CNRS, Institut de Physique et Chimie des Matériaux de Strasbourg UMR 7504, 23 rue du Loess, 67034 Strasbourg, France
[b] Dassault Aviation, 78 quai Marcel Dassault, 92552 Saint-Cloud, France
[c] University of Strasbourg - CNRS, ICube Laboratory UMR 7357, 23 rue du Loess, 67037 Strasbourg, France

ARTICLE INFO

Keywords:
Carbon nanotubes
Cobalt nanoparticles
Dielectric response
Density functional theory
First principles molecular dynamics

ABSTRACT

A new frontier in tuning the electromagnetic response of carbon-based materials, particularly carbon nanotubes, consists in adding metallic clusters or nanoparticles at their external surface. This allows to change optical, dielectric and magnetic properties with potential applications in electronics and telecommunications for aeronautics. By resorting to first principles dynamical simulations, we provide a microscopic picture of the interaction at finite temperature between a carbon nanotube and Co aggregates mimicking the experimental coverage. The electronic structure evolution provides the absorption spectrum and the dielectric function for comparison with experiments and guidelines for tuning these composite systems.

1. Introduction

A forefront activity in the field of materials for electronic and telecommunication applications oriented to aeronautics is the search for suitable composite systems to be used for electromagnetic shielding or absorbers to protect electronic devices and to reduce the human exposure against unwanted radiations. These materials are also foreseen to design new miniaturized antennas systems [1–3]. In this context, the main target for absorbers is the identification of the microscopic mechanisms, often occurring at an atomic-scale level, responsible for the electromagnetic absorption at the macroscopic scale by the permittivity and permeability spectra. From the spectral standpoint, such materials have to operate over an ever-increasing frequency range including the microwave domain (GHz range) and more recently the terahertz domain (0.3–10 THz) [4]. The wide range of possible systems that could potentially answer to these requirements is being narrowed down to accessible chemical elements, affordable realization costs and sustainability [5–8]. For these reasons, we focus here on single-walled carbon nanotubes (SW-CNT) coated with a Co nanoclusters as a prototype system currently explored for the specific applications mentioned above [9,10]. Since their discovery more than twenty years ago [11], CNTs in direct interaction with metallic atoms and nanoparticles have attracted a growing interest in a continuously growing range of applications for next-generation devices and systems [12]. Their acknowledged efficiency in terms of electronic and thermal transport, the relatively low production cost, and their controllable environmental impact at least to some extents are counterbalanced by the intrinsic difficulty in growing a specific nanotube in situ and in controlling their chirality [13]. The physical properties of a CNT can be tuned by adding heteroatoms or clusters at the surface [14,15], by substitution of C sites directly on the CNT network [16,17] or by encapsulating heteroatoms, molecules or clusters inside the CNT [18,19]. This can lead to new optical, electronic or magnetic properties according to the chemical nature of these heteroatoms [20–22]. In the microwave domain, Sui and coworkers [10] have shown that Co atoms deposited on CNTs allow to modulate the frequency response of composite polymer/CNT systems resulting in a shift of the absorption peak. Another example concerns the hydrogen functionalization of CNTs that induces changes in the THz power absorption spectrum measured by time-domain spectroscopy [23].

Yet, despite the intensive experimental activity of the last ten years, a detailed atomic-level knowledge of the mechanisms regulating the interaction of heteroatoms and clusters with CNTs is still lacking. Nonetheless, this fundamental knowledge is instrumental to design and tune the resulting macroscopic properties, and in particular the dielectric response of these composite materials. Starting from this rich background, in this work we resort to well benchmarked simulations tools and methods to investigate the behavior at finite temperature of SW-CNT decorated with a variable number of Co clusters mimicking the actual experimental coverage, which, ultimately, determines the sought macroscopic properties of these composite systems. The choice of coated CNTs [9,10], as opposed to CNTs encapsulating metallic

* Corresponding author.
E-mail address: boero@unistra.fr (M. Boero).

https://doi.org/10.1016/j.cartre.2024.100410
Received 20 August 2024; Received in revised form 3 October 2024; Accepted 4 October 2024
Available online 11 October 2024

atoms or clusters [19], is due to the fact that the production of these composite systems is less demanding than a growth of CNT around Co clusters or nanoparticles and the amount of metallic atoms coating the CNT can be better controlled, with clear advantages in term of feasibility and production costs.

By resorting to first principles molecular dynamics (FPMD) simulations, we aim at unraveling the underlying structural and the dynamically evolving electronic properties (global and local dipole, dielectric response, etc.) in the temperature range where these systems are expected to be operational. Furthermore, our objective is to compute the resulting complex dielectric function, directly obtained as a Fourier transform of the dipole autocorrelation function, over a broad frequency range covering the THz and infrared domains (10–3000 cm^{-1}). Quantitative comparison with available experimental results provide a solid background to assess the outcome of our simulations.

2. Methods

As a reference system, we considered a carbon nanotube of chirality (10,10) as a prototype of armchair system possessing conductivity properties, being stable over a rather wide range of temperature and currently used for chemisorption experiments [24–26]. This specific chirality is the one targeted also by our experimental counterpart within our academic–industrial collaboration. This does not exclude the possibility to study other chiralities and semimetallic CNTs, but, on one hand, this is beyond our scope and, on the other hand, would represent an additional huge computational workload. The simulated segment of this (10,10) CNT, shown in Fig. S1 (a) of the Supplementary Data, contains 240 C atoms, has a diameter of 13.50 Åand a length of 14.77 Å. This system is simulated inside an orthorhombic cell $a \times b \times c = 34.40 \times 34.40 \times 14.77$ $Å^3$ for an isolated CNT and $a \times b \times c = 42.33 \times 32.33 \times 14.77$ $Å^3$ for CNTs decorated with Co clusters on which periodic boundary conditions are applied. With this choice, the CNT is periodically repeated along the c axis whereas along the other two axes the large empty space ensures a good separation from repeated images and a space sufficient to accommodate the Co clusters detailed in the ongoing discussion. Before any dynamical simulation, the CNT, either pristine or decorated with Co nanoparticles, was fully relaxed to ensure a stable local minimum for the initial structure.

Concerning the Co nanoclusters, due to the poor literature available on structural data of these nanoobjects, we constructed a minimal nanoparticle composed of 12 Co atoms compatible with published data [27]. This cluster was first optimized at the DFT level described below and then equilibrated for about 15 ps in a microcanonical NVE ensemble, followed by a canonical NVT dynamics at 300 K lasting for 45 ps. In this NVT ensemble, only the last 35 ps were used for accumulating the dipole trajectory and making all the post-processing analysis, being the first 5 ps a mere equilibration stage from NVE to NVT. The equilibrated structure, shown in Fig. S1 (b) of the Supplementary Data, assumes a conformation compatible with the hexagonal closed-packed bulk Co [28] with bond lengths (2.25-2.29 Å) and angles ($\sim 60°$) of the triangular facets typical of this type of symmetry. As mentioned above, a spin-unrestricted description was adopted to check for possible spin-related issues (magnetic moment) of the Co nanocluster, evidencing an overall symmetric distribution of spin-up and spin-down distributions conferring a zero total spin to this type of Co nanocluster.

According to experimental indications about the coverage of typical CNTs both from the literature quoted above and data from our experimental partners, and considering the size of our Co nanoclusters, we can decorate our CNT with either three or four of them. This will be the guideline followed in the ongoing analysis.

All the simulations conducted here have been done within the FPMD approach according to the Car-Parrinello method [29] within the DFT framework [30]. In all the dynamical simulations, for the numerical integration of the equations of motion, a fictitious electron mass of 380 a. u. and a time step of 4 a. u. (0.097 fs) ensured good numerical control of the constants of motion. The specific DFT choice we made consists of the Becke [31] exchange and Lee–Yang–Parr [32] correlation functionals (BLYP), a choice that has already been benchmarked and used for simulating stand-alone CNTs and CNTs interacting with atoms and molecules [33]. The BLYP functional was complemented by the inclusion of van der Waals interactions according to the maximally localized Wannier functions [34] implementation [35,36]. The core-valence interaction was described by a norm-conserving numerical pseudopotential of the Troullier–Martins type [37] for C and a semi-core one of the Goedecker–Teter–Hutter type [38] for Co. Electronic wavefunctions are expanded on a plane wave basis set with a cut-off of 100 Ry (1360.57 eV) and the sampling of the Brillouin zone of the reciprocal space of the simulation cell was limited to the Γ point. The relatively large value of the cut-off has been selected to ensure an accurate description of the semi-core states included in the construction of the Co pseudopotential [38]. All calculations have been done in a spin-unrestricted approach. In all the canonical NVT simulations presented in the ongoing discussion, the temperature was controlled by a Nosé-Hoover thermostat chain [39]. Additional details will be given in the following paragraphs whenever needed to support the discussion. Simulations were performed with the CPMD package [40]. For convenience, we speak about IR-spectrum even if the lower-frequency part (10–300 cm^{-1}, representing about 10% of the whole spectrum) corresponds to the THz range.

3. Results and discussion

As a benchmark and reference for the case of Co-decorated CNT, we performed an NVT simulation at 300 K of the isolated (10,10) CNT. This simulation, after an initial equilibration of about 5 ps, lasted for 40 ps and during this time the total dipole moment $\mathbf{M}(t)$ was computed on-the-fly and accumulated to extract the infrared (IR) absorption spectrum as done and benchmarked in former works [41–43], namely as a Fourier transform of the dipole–dipole autocorrelation function $\langle \mathbf{M}(t+t')\mathbf{M}(t') \rangle$,

$$\alpha(\omega) = \frac{4\pi\omega \cdot \tanh(\beta\hbar\omega/2)}{3\hbar c V \cdot n(\omega)} \int_0^\infty e^{-i\omega t} \langle \mathbf{M}(t+t')\mathbf{M}(t') \rangle dt \quad (1)$$

where $\beta = 1/k_B T$, being T the temperature at which the simulation has been conducted and k_B the Boltzmann's constant, V the volume of the simulation cell, $\hbar$ the Planck's constant, c the speed of light and $n(\omega)$ the real part of the (complex) refractive index. Indeed, this formula gives the product $\alpha(\omega)\cdot n(\omega)$, directly comparable to the IR spectrum measured experimentally. The result of this analysis for the pristine (10,10) CNT is shown in panel (a) of Fig. 1. We notice that this spectrum agrees fairly well with the experimental results reported for CNTs [44,45]. More precisely, the peak at about 1590 cm^{-1}, attributed to the graphite-like G band and due to diametral oscillations of the CNT originating from the sp^2-hybridized C atoms orbitals [45], and the one around 880–900 cm^{-1} [44] more related to longitudinal oscillations along the nanotube axis are well reproduced by our simulations, although they have been shown to be dependent on the chirality of the CNT. Contrary to experiments, we do not have a CNT supported onto a solid substrate or embedded in a surrounding environment, thus the intrinsic flexibility of the isolated CNT at finite temperature confers some additional noise to the clean spectra detected experimentally. Yet, within the accuracy of our simulations, the quality of the IR spectrum ensures reliability to our approach.

Although we do not have neither sufficient statistics nor resolution to argue quantitatively about the very low frequency range, as shown in Fig. S3 of the Supplementary Data, a peak in the range 20–50 cm^{-1} (THz range) seems to be a systematic feature in the three spectra of increasing amplitude depending on the number of Co nanoclusters. This feature will be reflected in the dielectric response discussed later.

An analogous dynamical NVT simulation within the same spin-unrestricted approach was done for an isolated Co nanocluster. As

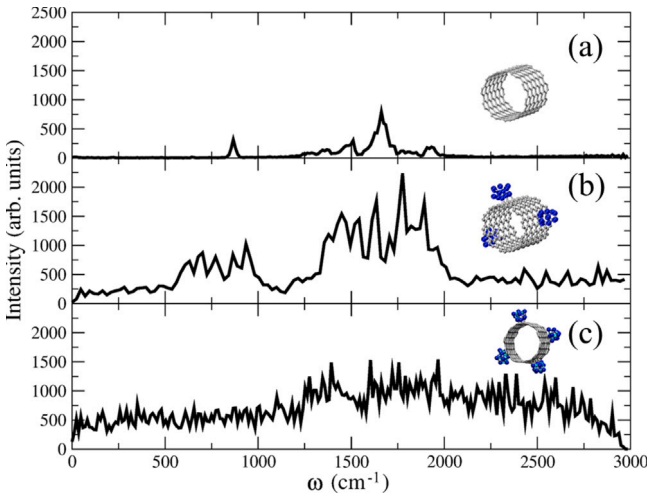

Fig. 1. Simulated IR absorption spectra for (a) the (10,10) carbon nanotube, (b) the same nanotube decorated with three Co nanoclusters, and (c) decorated with four Co nanoclusters. The inset figures are a graphic reminder of the system to which each spectrum refers and the color code is gray for C and blue for Co. (For interpretation of the references to color in this figure legend, the reader is referred to the web version of this article.)

mentioned in the methodological section, the total spin of twelve-atom cluster is equal to zero, indicating a non-magnetic state of our Co nanocluster. The IR absorption spectrum of this isolated Co nanocluster, shown in Fig. S2 of the Supplementary Data, was computed in the same way using the dipole accumulated along the last 35 ps of the 45 ps NVT dynamics mentioned in the former paragraph. Although the comparison with experiments is difficult because of the fact that we have here a single isolated Co nanocluster, whereas in experiments nanoparticles of different sizes on a solid support are realized, the spectrum we obtain is still compatible with the experimental outcome [46] although very noisy due to the free motion of the twelve-atom Co cluster. Moreover, as it can be seen from Fig. S2, the intensity is roughly two orders of magnitude smaller than the spectrum of the bare CNT, consistent with the general idea of a weak dielectric response.

Two systems were then prepared to simulate the (10,10) CNT interacting with three and four Co nanoclusters and corresponding to a coverage of ~ 15 % and ~ 20 %, respectively. After an initial relaxation and microcanonical NVE simulation, to check for the stability of the initial structure according to the protocol described in the methodological section, the two systems were brought to 300 K via canonical NVT simulations. These simulations lasted for 50 ps and the last 30 ps, where the system is well equilibrated and has already lost memory of the initial conditions, were used to accumulate statistics and extract the IR absorption spectra. The result is summarized in Fig. 1(b) and (c), respectively. A macroscopic effect induced by the presence of three Co nanoclusters is the fact that the overall amplitude of the spectrum increases of about a factor of two and becomes more noisy. The main peak of the *G* band around 1590 cm^{-1} spreads and split on a number of roughly equivalent peaks covering the range between 1300 and 2000 cm^{-1}. Analogously, the sharp peak at 880–900 cm^{-1} broadens and becomes a sequence of nearly equivalent peaks ranging from ~ 700 to 900 cm^{-1}. It is worth noting the enhancement of the amplitude of the spectrum in the lower frequency range (THz range), indicating that the system starts having an electromagnetic activity also at $\omega < 300$ cm^{-1}. This effects is further enhanced when four Co nanoclusters are introduced, as seen in panel (c) of Fig. 1, resulting in a very noisy IR spectrum. By looking at the atomistic mechanisms occurring during the canonical NVT dynamics, we noticed two main features to which the signal amplification and increase of the noise can be ascribed. The first one is that the Co clusters form chemical bonds with C atoms at the surface of the CNT, hence being chemisorbed, with bond lengths of 2.00–2.15 Å. This has then the effect of slowing down locally all the vibrational modes of the C atoms directly bound to these metallic nanocusters. A second effect is that at finite temperature (300 K in our case) these Co clusters are mobile and diffuse along the CNT by breaking and reforming these chemical bonds rather quickly with an average speed of 0.82±0.09 Å/ps corresponding to a diffusion coefficient of $5.8 \pm 0.2 \times 10^{-4}$ cm^2/s as illustrated in the panel (a) of Fig. 2.

This displacement is accompanied by fluctuations of the shape of the Co nanoclusters which do not undergo any Co–Co bond cleavage, thus keeping their size. By looking at the cross section of the CNT shown in Fig. 2(b), we remark that the heavy Co clusters induce large deformations on a relatively long time scale (about 4-5 ps) of the nanotube, thus contributing to a shift toward lower frequencies also of the *G* band with the effects observed in the IR spectrum of Fig. 1.

The increase of the noise on the spectrum and, at the same time, of the overall amplitude of the IR signal shown in Fig. 2(c) is the result of the addition of a fourth Co nanocluster to the (10,10) CNT. In the range 1300–2000 cm^{-1} we can barely recognize a set of dispersed peaks reminiscent of the *G* band of the pristine CNT, whereas the peak at 880–900 cm^{-1} is completely washed out by the dynamically interacting Co nanoclusters. This is accompanied by a more pronounced response in the region below 300 cm^{-1} (THz range). Yet, the diffusion of the Co nanoclusters, in this case of increased coverage, gives rise to another phenomenon, namely a coalescence of the Co clusters diffusing

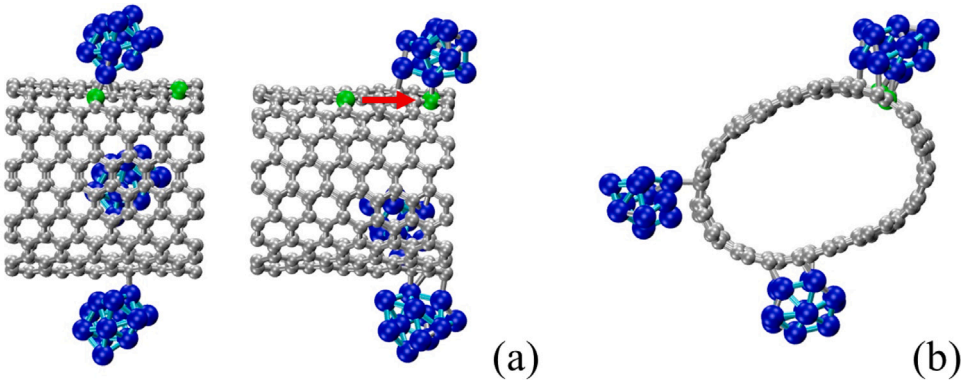

Fig. 2. Evolution of the (10,10) CNT decorated with three Co nanoclusters. (a) displacement of the Co nanoclusters during the NVT dynamics. The C atoms highlighted in green show the initial position of one of the three clusters (left) where a C–Co chemical bond exists and (right) displaced position assumed by this same Co nanocluster after 8.7 ps along the direction indicated by the arrow, where a new C–Co chemical bond has been created with the C site shown in green. Panel (b) shows a representative snapshot of the radial distortions occurring to the CNT as a consequence of the presence of Co nanoclusters bound to the external surface and diffusing on it. Apart from the C atoms evidenced in green, the same color code of former figures is used. (For interpretation of the references to color in this figure legend, the reader is referred to the web version of this article.)

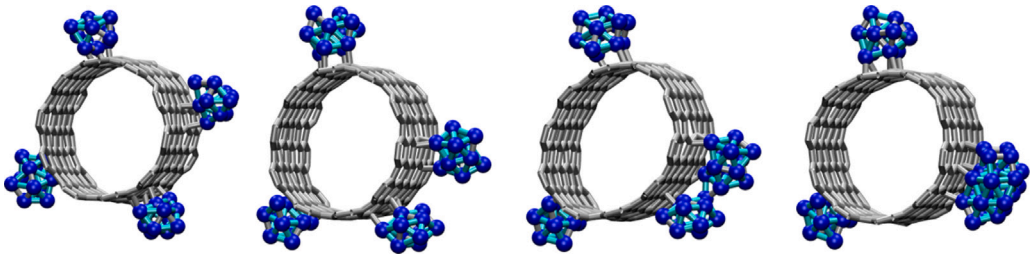

Fig. 3. Panels from let to right show the dynamical evolution of the four Co nanoclusters on the (10,10) CNT during our canonical NVT simulation resulting in the formation of larger Co cluster which remains stable on the time scale of our FPMD. The color code is the same used in former figures. (For interpretation of the references to color in this figure legend, the reader is referred to the web version of this article.)

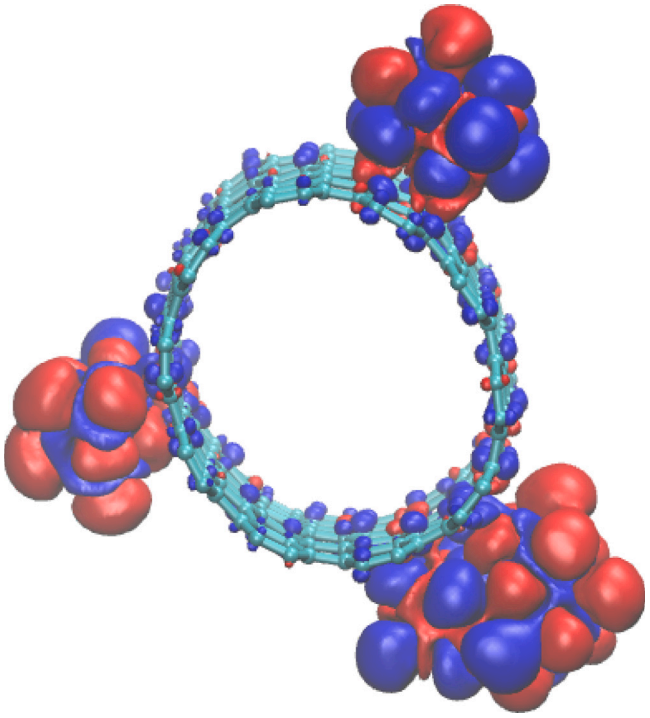

Fig. 4. Spin density distribution for the CNT system carrying four Co nanoclusters after the clusterization process discussed in the text and shown in the former figure. The total spin of the whole system is equal to zero as well as the partial spin of each single Co nanocluster decorating the CNT. The isosurfaces are shown at a value of $\pm 1.00 \times 10^{-3}$ $1/\text{Å}^3$ with the spin-up in red and the spin-down in blue. (For interpretation of the references to color in this figure legend, the reader is referred to the web version of this article.)

on the external surface of the CNT to form larger nanoclusters or nanoparticles, as illustrated in Fig. 3.

In about 20 ps, during our NVT dynamics, this clusterization process occurred for two of the four Co nanoclusters which meet each other during the random diffusion process discussed above. A practical consequence of the newly formed Co nanoparticle having a size double with respect to the original twelve-atom nanocluster is a slower diffusion of this larger object on the surface of the CNT. Yet, this alone is insufficient to hinder completely the process and to prevent further diffusion. We monitored also the evolution of the spin density of the system during this clusterization process. The final distribution is reported in Fig. 4 and shows clearly that the spin neutrality is kept all along the process, thus not involving the arising of undesired (or uncontrolled) magnetic moment.

The enhancement and remarkable change in the IR spectrum upon addition of Co clusters can be rationalized in terms of local modifications of the structure and related dipole moment on the CNT. As shown in Fig. S4 and S5 of the Supplementary data, the C atoms of the CNT forming chemical bonds with Co atoms undergo a significant elongation inducing a deformation up to the fourth neighbor. This translates also in an enhancement of the local dipole moment $|\mathbf{p}|$ whose distribution (Fig. S6), although broad due to the dynamical deformations, is centered at 0 D for both the longitudinal and radial values of the local $|\mathbf{p}|$, whereas pronounced peaks between 3.5 and 12.3 D arise in the longitudinal distribution, extending up to 15.7 D in the radial component. At the same time, the massive Co clusters reduce the deformations of the CNT conferring a reduced broadening to the distribution.

For a more direct comparison with macroscopic quantities of practical interest for the realization of these composite materials, we computed the complex dielectric function $\varepsilon(\omega) = \varepsilon_1(\omega) + i\varepsilon(\omega)$. The imaginary part can be obtained from Eq. (1),

$$\varepsilon_2(\omega) = \frac{2c \cdot \alpha(\omega) \cdot n(\omega)}{\omega} \tag{2}$$

which holds for a non-magnetic medium. This is indeed the case here, since we can neglect any dynamical permeability induced by the Co clusters, due to their low amount. Moreover, even if present, such a dynamically induced permeability is generally very low and restricted to a frequency domain below 10 GHz in the absence of applied magnetic fields and totally absent in the THz and IR range. The real part $\varepsilon_1(\omega)$ is given by the Kramers-Kronig dispersion formula

$$\varepsilon_1(\omega) = 1 + \frac{2}{\pi} P \int_0^{\infty} \frac{\omega' \cdot \varepsilon_2(\omega')}{\omega'^2 - \omega^2} d\omega' \tag{3}$$

with obvious notations and following a well assessed protocol [43]. The results of these calculations for the three systems studied in this work are reported in Fig. 5, along with the comparative plot of the dielectric loss tangent defined as $\text{tg}(\Delta) = \varepsilon_2(\omega)/\varepsilon_1(\omega)$.

The modifications over the whole frequency range, along with the amplification toward the low frequency interval below 300 cm^{-1}, reflect the discussion given above for the IR spectrum. The peak located between 20 and 50 cm^{-1} previously evidenced is further enhanced by the factor $1/\omega$ in Eq. (2), as shown in Fig. S7 of the Supplementary Data. We reiterate that we are at the limit of what we can appreciate within the simulation time scale of our study. Nonetheless, this qualitative trend is worthy of mention, being a systematic feature rather than a simple random numerical fluctuation. In particular, the dielectric loss tangent is helpful in evidencing the fact that the response is amplified, along with the low frequency window in which this enhancement is present, as a consequence of the inclusion of Co nanoparticles in the system. This, however, has to be taken with some care because of the diffusivity of Co clusters and nanoparticles occurring already at 300 K and which is likely to be enhanced at higher temperatures. Another point worthy of note is the fact that beside the physical and chemical nature of the atoms decorating the CNT, which have their own absorption and dielectric properties, the fact that these relatively massive objects form chemical bonds with the C atoms of the CNT results in a slowing down of the collective modes of all the C atoms bound to the Co nanoparticle or nanocluster. These collective modes are indeed the ones

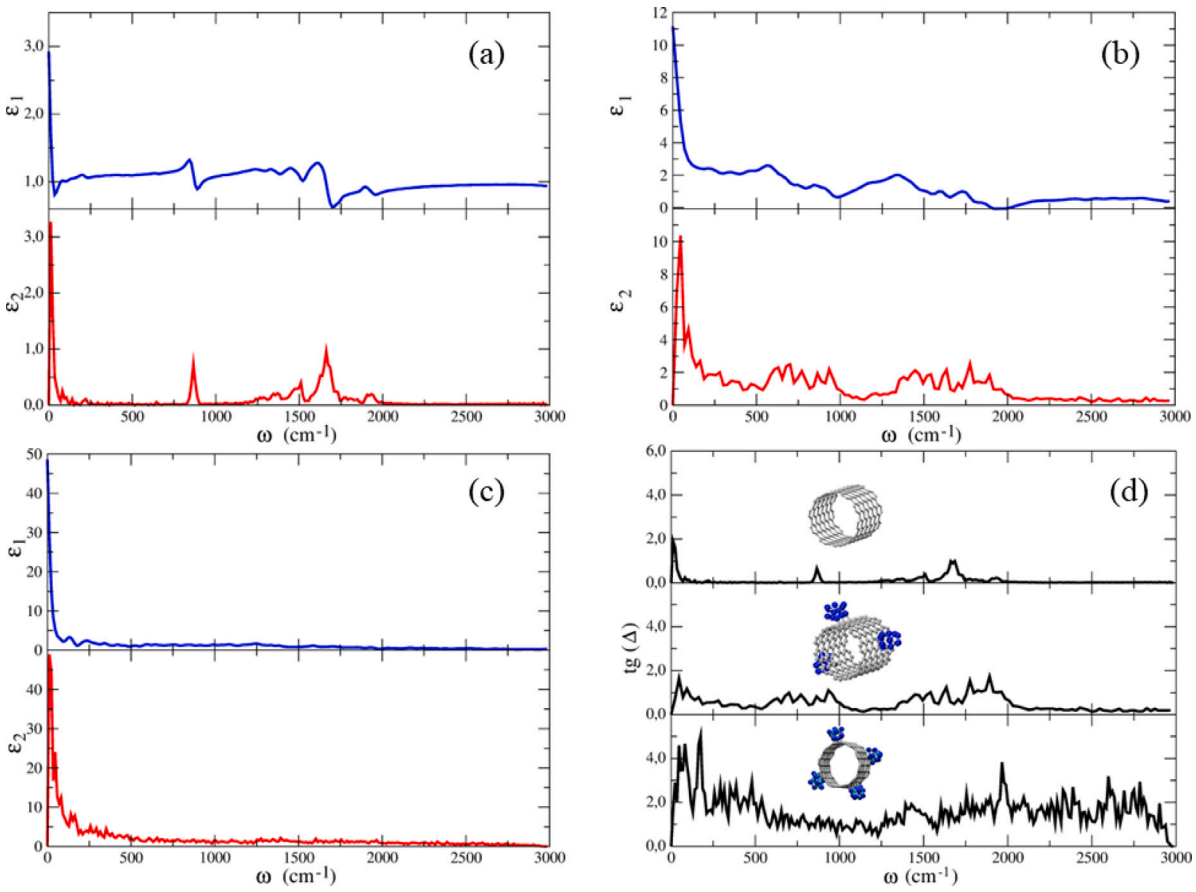

Fig. 5. Real (blue lines) and imaginary (red) part of the complex dielectric function for the bare (10,10) CNT (a) the same CNT decorated with three (b) and four (c) Co nanoclusters. Panel (d) shows the three dielectric loss tangent curves for these three systems with the same labeling and the inset figures are a reminder of the system to which they refer. (For interpretation of the references to color in this figure legend, the reader is referred to the web version of this article.)

responsible for the low frequency part of the IR spectrum and dielectric function, thus indicating that the nature of the electrostatic interaction between CNTs and decorating heteroatoms and the size of the clusters are two major ingredients in the tuning of the response of the composite material in the targeted frequency regime. The mobility observed at finite temperature for the Co nanoclusters decorating the CNT, although not affecting the overall dielectric response of the composite system, can represent a problem in real device applications. To mitigate this effect, a possible solution, still under experimental investigation, is to blend CNTs in a polymer matrix [47] prone to stabilize the system. Indeed, this is the subject of our ongoing study and will be the target of a forthcoming publication.

4. Conclusions

The present computational analysis aims at unraveling the processes occurring at finite temperature of a system composed of CNTs decorated with small amounts of Co organized in clusters (or nanoparticles). This type of composite materials is being pioneered as possible dielectrics in a wealth of applications including aeronautics and related electronics. To date, experiments are still difficult to interpret and accurate atomistic simulations still lacking. By resorting to FPMD modeling, we could provide a direct insight into the atomic structure and its evolution at finite temperature. The explicit inclusion of the electronic structure ant its evolution along rather long-lasting dynamical simulations allowed us to extract the dielectric response of this type of systems, evidencing the dependence of this measurable quantities on both the chemical nature of the system and the amount of Co added to trigger the absorption over a broad frequency range. We are aware that the microwave range is hard to reach due to the intrinsic difficulty of quantum-based simulations which are by their own nature bound to the ps time scale (e. g. a 300 ps simulation corresponds to a low-limit frequency of $\sim$ 3 GHz= 0.1 cm^{-1}). Nonetheless, this is a first attempt at pushing this type of modeling toward the limits of present high-performance computing architectures and massively parallel codes. A promising way to overcome the time scale limitations of this type of FPMD dynamical approaches, still at its pioneering stage, can be a deep-learning perturbation DFT [48] approach, although no guarantee can be presently given on its applicability to this type of complicated composite systems. The results obtained show that thermal stability problems can affect the microscopic organization of the system which however does not undergo disruption or chemical dissociation separating in an irreversible way the Co and the carbon-based components. Furthermore, our study can provide a guideline for a rational design of compounds suitable to these applications and a hint to stimulate molecular modeling in this rapidly evolving field.

CRediT authorship contribution statement

Icare Morrot-Woisard: Writing – review & editing, Validation, Investigation, Formal analysis, Data curation. **Emile K. Nguyen:** Investigation, Formal analysis. **Nicolas Vukadinovic:** Writing – review & editing, Validation, Supervision, Resources, Funding acquisition, Data curation, Conceptualization. **Mauro Boero:** Writing – original draft, Supervision, Software, Project administration, Methodology, Data curation,Conceptualization.

Declaration of competing interest

The authors declare the following financial interests/personal relationships which may be considered as potential competing interests: Icare Morrot-Woisard reports financial support was provided by LabCom MOLIERE - University of Strasbourg. If there are other authors, they declare that they have no known competing financial interests or personal relationships that could have appeared to influence the work reported in this paper.

Data availability

Data will be made available on request.

Acknowledgments

This work was granted access by GENCI (Grand Equipement National de Calcul Intensif), France under allocation DARI A016090692 and HPC Mesocenter at the University of Strasbourg funded by the Equipex Equip@Meso and the CPER Alsacalcul/Big Data, France. We acknowledge financial support from Agence de l'Innovation de Défense and Dassault Aviation under the LabCom MOLIERE, France. We are grateful to Guido Ori and Chrstophe Lefevre for insightful discussions.

Appendix A. Supplementary data

Supplementary material related to this article can be found online at https://doi.org/10.1016/j.cartre.2024.100410.

References

[1] X. Zheng, H. Zhang, Z. Liu, R. Jiang, X. Zhou, Functional composite electromagnetic shielding materials for aerospace, electronics and wearable fields, Mater. Today Commun. 33 (2022) 104498, http://dx.doi.org/10.1016/j.mtcomm.2022.104498.

[2] D. Munalli, G. Dimitrakis, D. Chronopoulos, S. Greedy, A. Long, Electromagnetic shielding effectiveness of carbon fibre reinforced composites, Composites B 173 (2019) 106906, http://dx.doi.org/10.1016/j.compositesb.2019.106906.

[3] Y. Bhattacharjee, S. Bose, Core-shell nanomaterials for microwave absorption and elctromagnetic interference shielding: A review, ACS Appl. Nano Mater. 4 (2021) 949–972, http://dx.doi.org/10.1021/acsanm.1c00278.

[4] S. Venkatachalam, K. Zeranska-Chudek, M. Zdrojek, D. Hourlier, Carbon-based terahertz absorbers: Materials, applications, and perspectives, Nano Select 1 (2020) 471–490, http://dx.doi.org/10.1002/nano.202000067.

[5] M.F.L. De Volder, S.H. Tawfick, R.H. Baughman, A.J. Hart, Carbon nanotubes: Present and future commercial applications, Science 339 (2013) 535–539, http://dx.doi.org/10.1126/science.1222453.

[6] H. Komatsu, T. Matsunami, Y. Sugita, T. Ikuno, Direct formation of carbon nanotube wiring with controlled electrical resistance on plastic films, Sci. Rep. 13 (2023) 2254, http://dx.doi.org/10.1038/s41598-023-29578-w.

[7] A. Abdulhameed, M.M. Halim, Electrical and thermal conductivity enrichment by carbon nanotubes: a mini-review, Emergent Mater. 6 (2023) 841–852, http://dx.doi.org/10.1007/s42247-023-00499-8.

[8] R. Girardello, S. Tasselli, N. Baranzini, R. Valvassori, M. de Eguileor, A. Grimaldi, Effects of carbon nanotube environmental dispersion on an aquatic invertebrate, hirudo medicinalis, PLoS ONE 10 (2015) e0144361, http://dx.doi.org/10.1371/journal.pone.0144361.

[9] Z. Dong, J. He, J. Wang, R. Li, J. Ma, Decorating carbon nanotubes with cobalt nanoparticles, Mater. Lett. 62 (2008) 4059–4061, http://dx.doi.org/10.1016/j.matlet.2008.06.017.

[10] J. Sui, C. Zhang, J. Li, Z. Yu, W. Cai, Microwave absorption and catalytic activity of carbon nanotubes decorated with cobalt nanoparticles, Mater. Lett. 75 (2012) 158–160, http://dx.doi.org/10.1016/j.matlet.2012.02.007.

[11] S. Ijima, Helical microtubules of graphitic carbon, Nature 354 (1991) 56–58, http://dx.doi.org/10.1038/354056a0.

[12] Y. Pan, Y. Chen, Y. Lin, P. Cui, K. Sun, Y. Liu, C. Liu, Cobalt nickel phosphide nanoparticles decorated carbon nanotubes as advanced hybrid catalysts for hydrogen evolution, J. Mater. Chem. A 4 (2016) 14675–14686, http://dx.doi.org/10.1039/C6TA06975D.

[13] L.-C. Qin, Determination of the chiral indices (*n*,*m*) of carbon nanotubes by electron diffraction, Phys. Chem. Chem. Phys. 9 (2007) 31–48, http://dx.doi.org/10.1039/B614121H.

[14] N. Wu, H. Lv, J. Liu, Y. Liu, S. Wang, W. Liu, Improved electromagnetic wave absorption of Co nanoparticles decorated carbon nanotubes derived from synergistic magnetic and dielectric losses, Phys. Chem. Chem. Phys. 18 (2016) 31542–31550, http://dx.doi.org/10.1039/C6CP06066H.

[15] C.T. Heish, J.Y. Lin, Electrochemical capacitance from carbon nanotubes decorated with cobalt oxide nanoparticles in alkali electrolyte, ECS Trans. 13 (2008) 73, http://dx.doi.org/10.1149/1.2998533.

[16] H. Inani, K. Mustonen, A. Markevich, E.-X. Ding, M. Tripathi, A. Hussain, C. Mangler, E.I. Kauppinen, T. Susi, J. Kotakoski, Silicon substitution in nanotubes and graphene via intermittent vacancies, J. Phys. Chem. C 123 (2019) 13136–13140, http://dx.doi.org/10.1021/acs.jpcc.9b01894.

[17] S.V. Boroznin, Carbon nanostructures containing boron impurity atoms: synthesis, physicochemical properties and potential applications, Mod. Electron. Mater. 8 (2022) 23–42, http://dx.doi.org/10.3897/j.moem.8.1.84317.

[18] M.A. Kazakova, A.S. Andreev, A.G. Selyutin, A.V. Ishchenko, A.V. Shuvaev, V.L. Kuznetsov, O.B. Lapina, J.-B. d'Espinose de Lacaillerie, Co metal nanoparticles deposition inside or outside multi-walled carbon nanotubes via facile support pretreatment, Appl. Surf. Sci. 456 (2018) 657–665, http://dx.doi.org/10.1016/j.apsusc.2018.06.124.

[19] H. Chen, W. Wang, L. Yang, L. Dong, D. Wang, X. Xu, D. Wang, J. Huang, M. Lv, H. Wang, A review of cobalt-containing nanomaterials, carbon nanomaterials and their composites in preparation methods and application, Nanomaterials 12 (2022) 2042, http://dx.doi.org/10.3390/nano12122042.

[20] K.C. Chin, A. Gohel, H.I. Elim, W. Ji, G.L. Chong, K.Y. Lim, C.H. Sow, A.T.S. Wee, Optical limiting properties of amorphous sixny and SiC coated carbon nanotubes, Chem. Phys. Lett. 383 (1) (2004) 72–75, http://dx.doi.org/10.1016/j.cplett.2003.11.007.

[21] P. Watts, W. Hsu, Verification of electromagnetic induction from Fe-filled carbon nanotubes, Appl. Phys. A 78 (2004) 79–83, http://dx.doi.org/10.1007/s00339-003-2194-5.

[22] Q. Wu, C. Qiu, T.-S. Low, Magnetic nanostructures grown on vertically aligned carbon nanotube templates, Nano Lett. 2 (2002) 161–164, http://dx.doi.org/10.1021/nl015675u.

[23] C. Kang, I.H. Maeng, S.J. Oh, S.C. Lim, K.H. An, Y.H. Lee, J.-H. Son, Terahertz optical and electrical properties of hydrogen-functionalized carbon nanotubes, Phys. Rev. B 75 (2007) 085410, http://dx.doi.org/10.1103/PhysRevB.75.085410.

[24] E. Targholi, M. Molaei, S. Mousavi-Khoshdel, (10,10) Single walled carbon nanotube consisted of chemisorbed oxygen atoms as a promising supercapacitor electrode material:A first principles study, Chem. Phys. Lett. 664 (2016) 96–100, http://dx.doi.org/10.1016/j.cplett.2016.10.018.

[25] M.S. Dresselhaus, G. Dresselhaus, R. Saito, A. Jorio, Raman spectroscopy of carbon nanotubes, Phys. Rep. 409 (2005) 47–99, http://dx.doi.org/10.1016/j.physrep.2004.10.006.

[26] T.W. Odom, J.L. Huang, P. Kim, C.M. Lieber, Structure and electronic properties of carbon nanotubes, J. Chem. Phys. B 104 (2000) 2794–2809, http://dx.doi.org/10.1021/jp993592k.

[27] J. C., A. Martinez, M. Castro, D.R. Salahub, Structure and properties of cobalt clusters up to the tetramer: A density-functional study, Phys. Rev. B 55 (1977) 10905–10921, http://dx.doi.org/10.1103/PhysRevB.55.10905.

[28] W. Betteridge, The properties of metallic cobalt, Prog. Mater. Sci. 24 (1980) 51–142, http://dx.doi.org/10.1016/0079-6425(79)90004-5.

[29] R. Car, M. Parrinello, Unified approach for molecular dynamics and density-functional theory, Phys. Rev. Lett. 55 (22) (1985) 2471–2474, http://dx.doi.org/10.1103/PhysRevLett.55.2471.

[30] W. Kohn, L.J. Sham, Self-consistent equations including exchange and correlation effects, Phys. Rev. 140 (4A) (1965) A1133–A1138, http://dx.doi.org/10.1103/PhysRev.140.A1133.

[31] A.D. Becke, Density-functional exchange-energy approximation with correct asymptotic behavior, Phys. Rev. A 38 (6) (1988) 3098–3100, http://dx.doi.org/10.1103/PhysRevA.38.3098.

[32] C. Lee, W. Yang, R.G. Parr, Development of the colle-salvetti correlation-energy formula into a functional of the electron density, Phys. Rev. B 37 (2) (1988) 785–789, http://dx.doi.org/10.1103/PhysRevB.37.785.

[33] R. Scipioni, M. Pumera, M. Boero, Y. Miyahara, T. Ohno, Investigation of the mechanism of absorption of β-nicotinamide adenine dinucleotide on single-walled carbon nanotubes, J. Phys. Chem. Lett. 1 (2010) 122–125, http://dx.doi.org/10.1021/jz9000714.

[34] N. Marzari, A.A. Mostofi, R.Y. Jonathan, I. Souza, D. Vanderbilt, Maximally localized wannier functions: Theory and applications, Rev. Mod. Phys. 84 (2012) 1419–1475, http://dx.doi.org/10.1103/RevModPhys.84.1419.

[35] P.L. Silvestrelli, Van der Waals interactions in DFT made easy by wannier functions, Phys. Rev. Lett. 100 (2008) 053002, http://dx.doi.org/10.1103/PhysRevLett.100.053002.

[36] T. Ikeda, M. Boero, Role of van der waals corrections in first principles simulations of alkali metal ions in aqueous solutions, J. Chem. Phys 143 (2015) 194510, http://dx.doi.org/10.1063/1.4935932.

[37] N. Troullier, J.L. Martins, Efficient pseudopotentials for plane-wave calculations, Phys. Rev. B 43 (3) (1991) 1993–2006, http://dx.doi.org/10.1103/PhysRevB.43.1993.

[38] S. Goedecker, M. Teter, J. Hutter, Separable dual-space Gaussian pseudopotentials, Phys. Rev. B 54 (3) (1996) 1703–1710, http://dx.doi.org/10.1103/PhysRevB.54.1703.

[39] G.J. Martyna, M.L. Klein, M. Tuckerman, Nosé-hoover chains: The canonical ensemble via continuous dynamics, J. Chem. Phys. 97 (1992) 2635–2643, http://dx.doi.org/10.1063/1.463940.

[40] CPMD, Copyright IBM Corp. 1990–2022, copyright MPI für Festkörperforschung Stuttgart 1997–2001. Available on GitHub under MIT License, [link] URL https://github.com/OpenCPMD.

[41] P.L. Silvestrelli, M. Bernasconi, M. Parrinello, Ab initio infrared spectrum of liquid water, Chem. Phys. Lett. 277 (1997) 7725–7729, http://dx.doi.org/10.1016/S0009-2614(97)00930-5.

[42] D.A. Schmidt, R. Scipioni, M. Boero, Water solvation properties: An experimental and theoretical investigation of salt solutions at finite dilution, J. Phys. Chem. A 113 (2009) 7725–7729, http://dx.doi.org/10.1021/jp9016932.

[43] K. Ishisone, G. Ori, M. Boero, Structural, dynamical, and electronic properties of the ionic liquid 1-ethyl-3-methylimidazolium bis(trifluoromethylsulfonyl)imide, Phys. Chem. Chem. Phys. 24 (2022) 9597–9607, http://dx.doi.org/10.1039/D2CP00741J.

[44] K. Sbai, A. RahmaniH, H. Chadli, J.-L. Bantignies, P. Hermet, J.-L. Sauvajol, Infrared spectroscopy of single-walled carbon nanotubes, J. Phys. Chem. B 110 (2006) 12388–12393, http://dx.doi.org/10.1021/jp0574504.

[45] N. Kouklin, M. Tzolov, D. Straus, A. Yin, J.M. Xu, Infrared absorption properties of carbon nanotubes synthesized by chemical vapor deposition, Appl. Phys. Lett. 85 (2004) 4463–4465, http://dx.doi.org/10.1063/1.1812837.

[46] A. Bigotto, V. Galasso, G. De Alti, Infrared spectra and normal vibrations of cobalt(II), nickel(II) and palladium(II) complexes with N,N'-ethylenebis(acetylacetoneimine), Spectrochim. Acta A 28 (8) (1972) 1581–1591, http://dx.doi.org/10.1016/0584-8539(72)80129-6.

[47] C. Pramanik, J.R. Gissinger, S. Kumar, H. Heinz, Carbon nanotube dispersion in solvents and polymer solutions: Mechanisms, assembly, and preferences, ACS Nano 11 (12) (2017) 12805–12816, http://dx.doi.org/10.1021/acsnano.7b07684.

[48] H. Li, Z. Tang, J. Fu, W.-H. Dong, N. Zou, X. Gong, W. Duan, Y. Xu, Deep-learning density functional perturbation theory, Phys. Rev. Lett. 132 (2024) 096401, http://dx.doi.org/10.1103/PhysRevLett.132.096401, URL https://link.aps.org/doi/10.1103/PhysRevLett.132.096401.